Hydrology Research

Hydrology Research Vol 54 No 10, 1281 doi: 10.2166/nh.2023.191

Hydrodynamics and sediment transport in Poyang Lake under the effects of wind and backflow

Hongwu Tang[a,b], Yang Yu[a], Saiyu Yuan[a,b,*], Zhipeng Li[a], Hao Cao[a], Chenyu Jiang[c] and Carlo Gualtieri[d]

[a] The National Key Laboratory of Water Disaster Prevention, Hohai University, Nanjing 210098, China
[b] Key Laboratory of Hydrologic-cycle and Hydrodynamic System of Ministry of Water Resources, Hohai University, Nanjing 210098, China
[c] Water Conservancy Development Research Center of Taihu Basin Authority of Ministry of Water Resources, Shanghai 200434, China
[d] Department of Civil, Architectural and Environmental Engineering (DICEA), University of Naples Federico II, Naples 80125, Italy
*Corresponding author. E-mail: yuansaiyu@hhu.edu.cn

ABSTRACT

The ecology of the aquatic environment in Poyang Lake, the largest fresh lake in China, is notably impacted by the backflow from the Yangtze River, which conveys a high flux of sediments. This study employs a widely recognized numerical model to replicate the backflow in 2007 (the strongest backflow after the operation initiation of the Three Gorges Dam) to investigate the contributions of wind and backflow to the sediment transport process. The results show that the influences of wind and backflow on flow patterns and sediment transport processes have significant spatial heterogeneity. In the narrow waterway leading to the central lake area, hydrodynamics is mainly driven by backflow. Conversely, the hydrodynamics of the open expanse of the lake is primarily influenced by wind forces. Dominant wind leads to the formation of gyres, which significantly alter flow paths and push sediment into the upstream areas. As a result, the suspended sediment area expands at an average rate of 20.1–21.3 km^2 daily, marking a 75–85% surge compared to the no wind condition (11.5 km^2). The study facilitates a deeper understanding of sediment transport processes in large lakes.

Key words: backflow, Poyang Lake, sediment transport, wind force, Yangtze River

HIGHLIGHTS

- Wind causes large gyres during the backflow period.
- Wind-induced current could modify the lake mainstream direction.
- Wind promotes sediment movement.

GRAPHICAL ABSTRACT

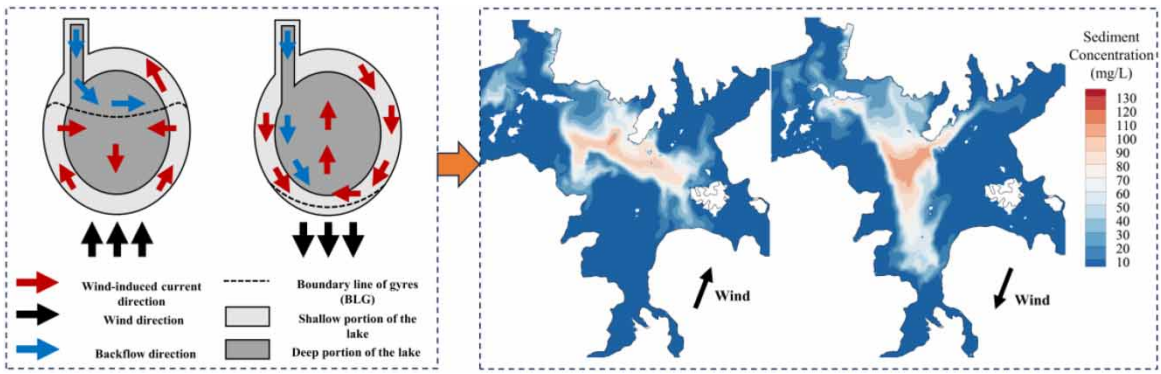

INDEX OF ABBREVIATIONS

BLG Boundary line between gyres
MODIS Moderate Resolution Imaging Spectroradiometer

NNE North-Northeast
RSM Resuspended sediments from the bed by sand mining
SSW South-Southwest
SYR Sediments originating from the Yangtze River
TGD Three Gorges Dam

INTRODUCTION

Backflow, the temporary reversal of discharge at a lake's outlet, plays a pivotal role in dictating flow and transport dynamics within many interconnected river–lake systems (Li *et al.* 2017, 2020). One notable instance of such a system is formed by the confluence of the Yangtze River and Poyang Lake – the former being China's largest river and the latter its largest freshwater lake (Wang *et al.* 2015; Liu *et al.* 2020; Tang *et al.* 2020). Due to the asynchronicity in their flooding seasons, backflow from the Yangtze River to Poyang Lake is frequent, particularly from July to October (Hu *et al.* 2007; Yang *et al.* 2016). The backflow from the Yangtze River to Poyang Lake typically persists for several days, sometimes reaching up to 40 days each year (Guo *et al.* 2012). This phenomenon not only propels sediments but also facilitates the migration of fish species from the Yangtze River to Poyang Lake (Wang *et al.* 2019, 2020). Effectively monitoring and evaluating these backflow events in Poyang Lake is crucial for understanding the lake's evolving water environment and material exchange dynamics, offering a solid scientific foundation for its holistic management (Zhang *et al.* 2016; Liu *et al.* 2017).

Data mining techniques with time series and remote sensing for the ecological monitoring of lakes have emerged as a significant contribution to protect the aquatic environment (Li *et al.* 2019; Khan *et al.* 2019a; Deoli *et al.* 2022). Furthermore, satellite monitoring has proven indispensable in investigating sediment transport within river and lake systems (Khan *et al.* 2019b; Ayele *et al.* 2021; Kumar *et al.* 2022). Utilizing MODIS monitoring, research into the backflow phenomenon consistently demonstrated extensive sediment transport throughout the lake (Wu *et al.* 2007; Chen *et al.* 2014; Mu *et al.* 2020). Cui *et al.* (2009), through their analysis of MODIS remote sensing imagery from 2004 to 2005, discerned that sediment driven by backflow from the northern channel impacted not only the northern portion of the lake but also its central and southern regions. In a parallel vein, Jiang *et al.* (2021) employed an innovative algorithm to pinpoint the scope and timing of backflow, concurring with Cui *et al.*'s (2009) findings on sediment movements toward Poyang Lake's upstream. In addition to image-based monitoring, some researchers have analyzed the effects of backflow-driven sediment movement. Ma *et al.* (2003) highlighted the backflow's pivotal role in sediment deposition in northern Poyang Lake, identifying significant sediment buildup rates between 1.6 and 3.1 cm/year, primarily attributed to this phenomenon. Notably, nutrient and pollutant distributions within Poyang Lake are swayed by backflow dynamics, given their bearing on water residence durations (Wu *et al.* 2007; Li *et al.* 2014).

While MODIS images allow for observation of the sediment movement path influenced by backflow, their utility is curtailed by the frequent cloud cover in the study area (Cui *et al.* 2009). To elucidate sediment transport dynamics during backflow episodes, Tang *et al.* (2015) employed the EFDC hydrodynamic model, demonstrating a flow direction from the northern inlet channel into the lake's eastern bay after backflow onset. Similarly, Li *et al.* (2017) utilized hydrodynamic and particle tracking models to highlight the disruption of Poyang Lake's typical northward flow by backflow, resulting in a southward mass movement. Notably, particle transport distances vary across the lake, with particles in the northern channel generally traveling farther than those in the central and southern regions.

Nevertheless, some inconsistencies arise when juxtaposing these insights with MODIS data. For instance, certain findings (Li *et al.* 2017) differ from MODIS-based observations (Cui *et al.* 2009) in terms of sediment transport distances. During the longest duration (27 days) or highest cumulative volume of backflow (1.2×10^{10} m^3), particles from the northern channel move within a range of 10–15 km and primarily concentrated near the center of the lake (Li *et al.* 2017). In contrast, MODIS data from 2004 suggested sediment transport distances of approximately 40–50 km within an 8-day span and 2.7×10^9 m^3 volume of backflow (Cui *et al.* 2009). These discrepancies underscore the importance of factors like wind in lake mixing dynamics, necessitating more comprehensive exploration.

Numerous studies underscore the profound influence of wind-driven forces on both lake dynamics and material transport. This influence is especially pronounced in shallow lakes, with Poyang Lake serving as a prime exemplar (Zou *et al.* 2020). Yao *et al.* (2016) elucidated that wind-driven forces exerted a greater impact on circulation within Poyang Lake's eastern sub-lakes than either inflows or outflows. In a distinct study, Wang *et al.* (2020) executed simulations on the dispersion of copper (Cu) particles within Poyang Lake, giving particular emphasis to the synergistic effects of wind dynamics. Their

findings underscored the profound impact of wind-induced currents on inflow, resulting in the initiation of horizontal circulation patterns. Yao *et al.* (2019) engaged in simulations assessing lake flow fields under wind influence. Their findings indicated that, at subdued wind velocities, a north-northeast wind direction augments the accumulation of particulates within the lake's eastern bay.

Collectively, these investigations indicated that sediment transport during backflow was influenced not only by the backflow itself but also by the wind. Owing to the shallow nature of Poyang Lake, its water flow is especially sensitive to wind (Yao *et al.* 2019). Wind generates circulation patterns and has the potential to markedly affect material transport within the lake (Liu *et al.* 2016). Given the complexity of these dynamics, future research should investigate such interplays. In the present study, a numerical model was applied to investigate Poyang Lake's hydrodynamics and sediment transport, considering the effect of both backflow and wind. Our primary objectives are to (1) identify the spatial and temporal variations of hydrodynamics influenced by backflow and wind and (2) clarify the effects of wind on sediment transport. This study can provide a basis for future management of lakes and aquatic environmental governance.

STUDY AREA AND DATA

Study area

Poyang Lake (28°4′–29°46′N, 115°49′–116°46′E; China), located in northern Jiangxi Province and on the southern bank of the middle and lower reaches of the Yangtze River (Figure 1(a)), is the largest freshwater lake in China and the largest natural flood regulation and storage area in the Yangtze River Basin (Feng *et al.* 2012; Yuan *et al.* 2018). Poyang Lake is an important water source in the middle and lower reaches of the Yangtze River as well as China's largest freshwater fish-producing area, an internationally important wetland, and a world-famous wintering habitat for migratory birds. Ninety-five percent of the world's white cranes and the world's largest group of geese overwinter here (Mei *et al.* 2015).

The elevation of the lakebed generally decreases from south (upstream) to north (downstream), with a difference of 6.5 m (Li *et al.* 2014). Eighty-five percent of the Poyang Lake area exhibits a water depth lower than 6 m during the flood season, indicating that the lake is generally shallow. Poyang Lake joins the Yangtze River at the Hukou station through a narrow and deep outflow channel called the Duchang–Hukou outflow channel (Figure 1), which is 3–5 km wide and located in the northern part of the lake (Yuan *et al.* 2021; Xu *et al.* 2022). The southern part is the main lake, which is 133 km in length and 74 km at its widest. Shallow floodplains are distributed to the north of the main lake (Wu *et al.* 2007). Poyang Lake features a total of five hydrological stations that are positioned along its course from upstream to downstream. These stations, in sequential order, are Kangshan, Tangyin, Duchang, Xingzi, and Hukou.

Poyang Lake contains five inflow rivers, namely, the Xiushui River, Ganjiang River, Fuhe River, Rao River (its branches are the Le'an River and Changjiang River), and Xinjiang River. The Yangtze River discharge and catchment inflows vary considerably throughout the year, with a time lag between the peak discharge of the Yangtze River (July–September) and the maximum catchment inflows (April–June). In Poyang Lake, the flood season begins in April, and the increase in upstream inflows causes the lake level to rise. Before July, the outflow from Poyang Lake can quickly enter the Yangtze River. However, during the flood season of the Yangtze River from July to September, the river water level rises, resulting in backflow (Shankman *et al.* 2006; Yao *et al.* 2018). Under the combined influences of the five inflows and the Yangtze River backwater flow, the hydrodynamics and sediment transport process in Poyang Lake are very complex and subject to notable changes in time and space.

Hydrodynamic model

The finite-volume coastal ocean model (FVCOM) is a non-structural grid model. In a Cartesian coordinate system, the FVCOM solves the following momentum and mass conservation equations (Chen *et al.* 2007):

$$\begin{cases} \dfrac{\partial u}{\partial t}+\dfrac{\partial u}{\partial x}+v\dfrac{\partial u}{\partial y}+w\dfrac{\partial u}{\partial z}-fv=-\dfrac{1}{\rho}\dfrac{\partial P}{\partial x}+\dfrac{\partial}{\partial z}\left(K_m\dfrac{\partial u}{\partial z}\right)+F_u \\ \dfrac{\partial v}{\partial t}+\dfrac{\partial v}{\partial x}+v\dfrac{\partial v}{\partial y}+w\dfrac{\partial v}{\partial z}+fu=-\dfrac{1}{\rho}\dfrac{\partial P}{\partial y}+\dfrac{\partial}{\partial z}\left(K_m\dfrac{\partial v}{\partial z}\right)+F_v \\ \dfrac{\partial P}{\partial z}=-\rho g \end{cases} \quad (1)$$

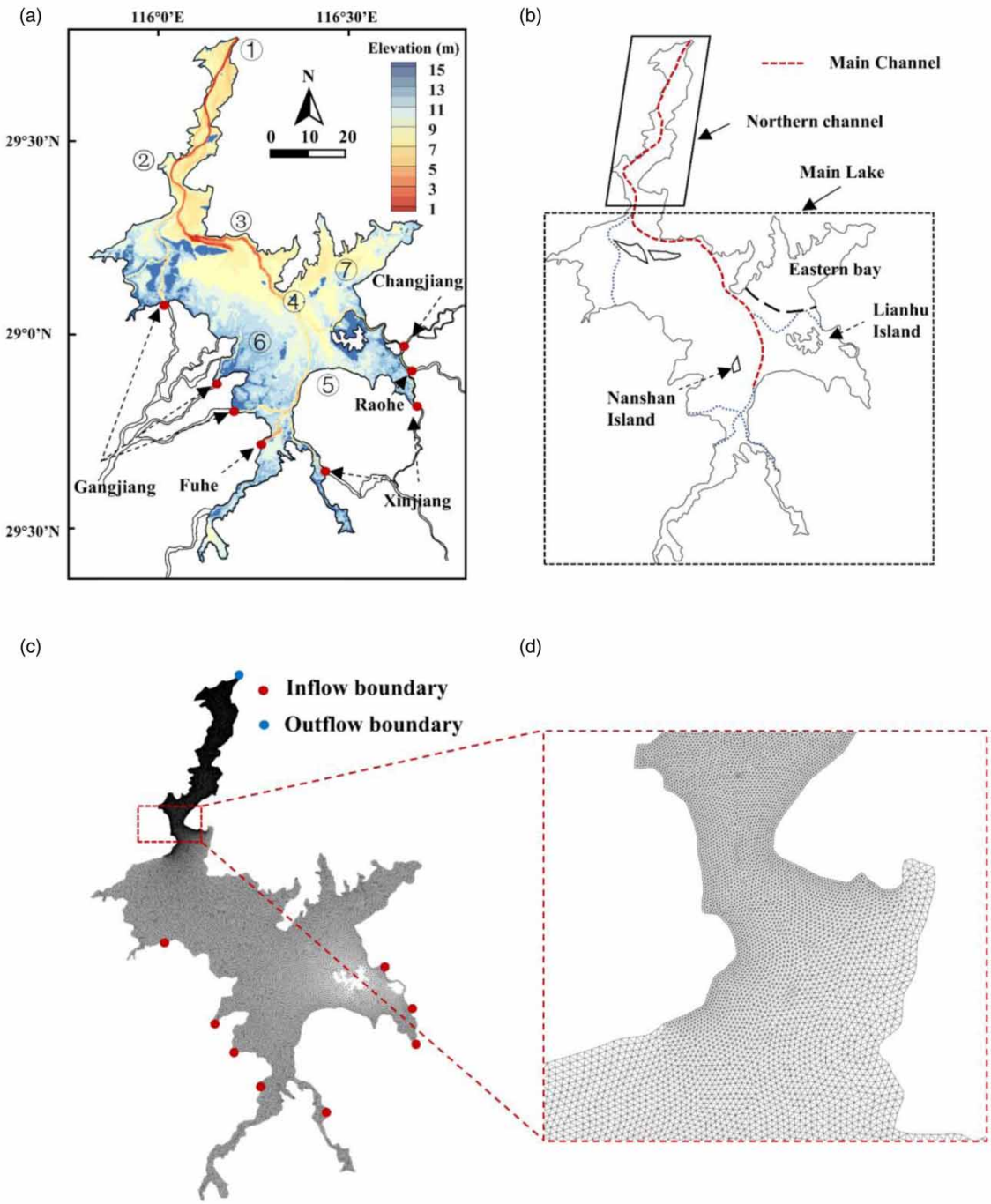

Figure 1 | Study site: (a) Contour of water depth of Poyang Lake and hydrological stations: ① Hukou; ② Xingzi; ③ Duchang; ④ Tangyin; and ⑤ Kangshan. Note that ⑥ and ⑦ are the interest points located in the western floodplain and eastern bay, respectively. (b) Distribution of the Main Channel, the Northern Channel, and the Main Lake. (c) The grid spacing distribution of the study area. (d) The enlarged view of the grid at the Xingzi–Duchang channel.

where x, y, and z are the east, north, and vertical coordinates, respectively; u, v, and w are the velocity components along the x, y, and z directions, respectively; ρ is the water density; P is the pressure; f is the Coriolis force parameter; g is the acceleration of gravity; K_m is the vertical eddy viscosity coefficient; and F_u and F_v are horizontal momentum diffusion terms.

The surface and bottom boundary conditions for u, v, and w (Chen *et al.* 2003) are:

$$K_m\left(\frac{\partial u}{\partial z}, \frac{\partial v}{\partial z}\right) = \frac{1}{\rho_o}(\tau_{sx}, \tau_{sy}), w = \frac{\partial \zeta}{\partial t} + u\frac{\partial \zeta}{\partial x} + v\frac{\partial \zeta}{\partial y} + \frac{E-P}{\rho}, \text{ at } z = \zeta(x, y, t) \tag{2}$$

$$K_m\left(\frac{\partial u}{\partial z}, \frac{\partial v}{\partial z}\right) = \frac{1}{\rho_o}(\tau_{bx}, \tau_{by}), w = -u\frac{\partial H}{\partial x} - v\frac{\partial H}{\partial y}, \text{ at } z = -H(x, y) \tag{3}$$

where $(\tau_{sx}, \tau_{sy}) = C_{sd}\rho_a U_{10}(U_{10x}, U_{10y})$ and $(\tau_{bx}, \tau_{by}) = C_{bd}\rho_w\sqrt{u^2+v^2}(u, v)$ are the x and y components of the surface wind and bottom stresses, respectively; ρ_a and ρ_w are air and water density, respectively; U_{10} is 10-m height wind speed; U_{10x} and U_{10y} are the x and y components, respectively; ζ is the height of the free surface; H is the bottom depth (relative to $z = 0$); and P and E denote precipitation and evaporation, respectively. The surface drag coefficient C_{sd} was set equal to 0.0012 considering both shallow lake and low wind speed of no larger than 11 m/s; the bottom drag coefficient C_{bd} was determined by matching a logarithmic bottom layer to the model at a certain height above the bottom (Chen *et al.* 2003). The sediment module of the FVCOM model was improved based on the ROMS_SED sediment transport model, and the advection–diffusion equation was adopted to calculate the suspended sediment concentration:

$$\frac{\partial C}{\partial t} + \frac{\partial (uC)}{\partial x} + \frac{\partial (vC)}{\partial y} + \frac{\partial (w - w_i)C}{\partial z} = \frac{\partial}{\partial x}\left(A_h\frac{\partial C}{\partial x}\right) + \frac{\partial}{\partial y}\left(A_h\frac{\partial C}{\partial y}\right) + \frac{\partial}{\partial z}\left(K_h\frac{\partial C}{\partial z}\right) \tag{4}$$

where C is the suspended sediment concentration; A_h and K_h are horizontal and vertical diffusion coefficients, respectively; and w_i is the settling velocity of the ith sediment type. According to the Hydrological Almanac, the suspended sediment of the Yangtze River has a mean grain size of 6 μm, and the resuspended sediment from the Poyang outlet has a mean grain size of 1 μm. K_m and K_h can be parameterized using the Mellor & Yamada (1982) level 2.5 (MY-2.5) turbulent closure model, as modified by Galperin *et al.* (1988). The horizontal eddy diffusion coefficient for momentum was calculated using the Smagorinsky (1963) eddy parameterization method.

The unstructured triangular grid adopted by the FVCOM can meet the requirement of geometric flexibility to fit the complex shorelines of the study domain. The study domain comprises the narrow outflow channel and the open lake area, and different spatial resolutions are needed. The triangles in the Duchang–Hukou channel had a spatial resolution of less than 150 m, whereas those in the open lake area had a spatial resolution ranging from approximately 300 to 400 m. This indicates that the level of detail in the triangulation was higher in the channel compared to the open lake area (Figure 1). The model encompassed a total of 70,458 triangles with 36,687 node points. The angles of each triangle element were limited to between 30° and 130°, and the number of triangular elements at each node was limited to 8 to ensure the mesh quality.

The model adopted a 60-d cold start before the backflow period to ensure the hydrodynamics simulation accuracy during the backflow period. The inflow boundary comprised the five upstream rivers and the interval flow. The Hukou station was considered the outlet boundary before the backflow period ($Q > 0$ m^3/s) but was considered the inlet boundary ($Q < 0$ m^3/s) during the backflow period. The observed water level at Kangshan was adopted as the initial water level of the whole study domain, and the initial velocity was set to 0. The time step for the external mode was set to 0.3 s in this model and that for the internal mode was set to 3.0 s.

Model data

The average daily observed inflows at eight locations (Figure 1(a)) in Poyang Lake and the observed water level at Hukou were used as boundary conditions for the hydrodynamic model. The average daily river discharge at Hukou and the average daily water level at the Xingzi, Duchang, Tangyin, and Kangshan stations in Poyang Lake were used to verify the model results. In addition, the distribution of suspended sediments caused by sand mining and backflow was derived from MODIS surface reflectance data (MOD09) collected in July and August from 2003 to 2007.

Simulated scenarios

This study included a series of simulations comprising seven distinct scenarios with various hydrological and wind conditions, as shown in Table 1. The initial three scenarios (Cases 1–3) aimed to model the backflow processes, without the influence of wind, during the years 2003, 2004, and 2007. Subsequently, three additional scenarios (Cases 4–6) were

Table 1 | Modelling scenarios under the combination of different backflow amount and wind field

Case	Year	Backflow amount (10^9 m^3)	Wind speed (m/s)	Wind direction
Case 1	2003	2.67	0	–
Case 2	2004	2.77	0	–
Case 3	2007	4.522	0	–
Case 4	2003	2.67	4.3	SSW
Case 5	2004	2.77	4.3	SSW
Case 6	2007	4.522	4.3	SSW
Case 7	2007	4.522	4.3	NNE

constructed to simulate the effect of SSW wind on the backflow processes during the same years. Finally, Case 7 was devised to evaluate the impact of NNE wind on the backflow processes in 2007, which corresponded to the highest substantial amount of backflow observed since the completion of the Three Gorges project.

The measured average wind speeds and directions in these cases at the Boyang station were statistically analyzed (Figure 2). The most common dominant wind direction was SSW. The average wind speed was 4.3 m/s, and the frequency was 48%. The dominant wind with a wind speed of 4.3 m/s was selected as the computational boundary condition in these cases.

Two main sources of sediments into Poyang Lake during the backflow period were identified, namely, sediments originating from the Yangtze River (SYR) conveyed by the backflow process and sediments resuspended from the bed by sand mining (RSM). SYR could be represented by the sediment data at the Hukou station, which was recorded by the Changjiang Water Resources Commission. Cui *et al.* (2013) suggested that the suspended sediment concentration could be estimated by MODIS images since they found a favorable regression function between the resuspended sediment concentration due to sand mining and the red band reflectance (R) of MODIS images:

$$\mathrm{RSM} = -7.6 + 634.9 \times R - 11,\ 152.1 \times R^2 + 69,\ 511.8 \times R^3 \tag{5}$$

Thus, the spatial RSM distribution for the initial condition could be obtained with this equation. In Case 1, MODIS remote sensing data before backflow (4 July 2003) and the initial conditions of sediment retrieval by MODIS remote sensing are shown in Figure 3.

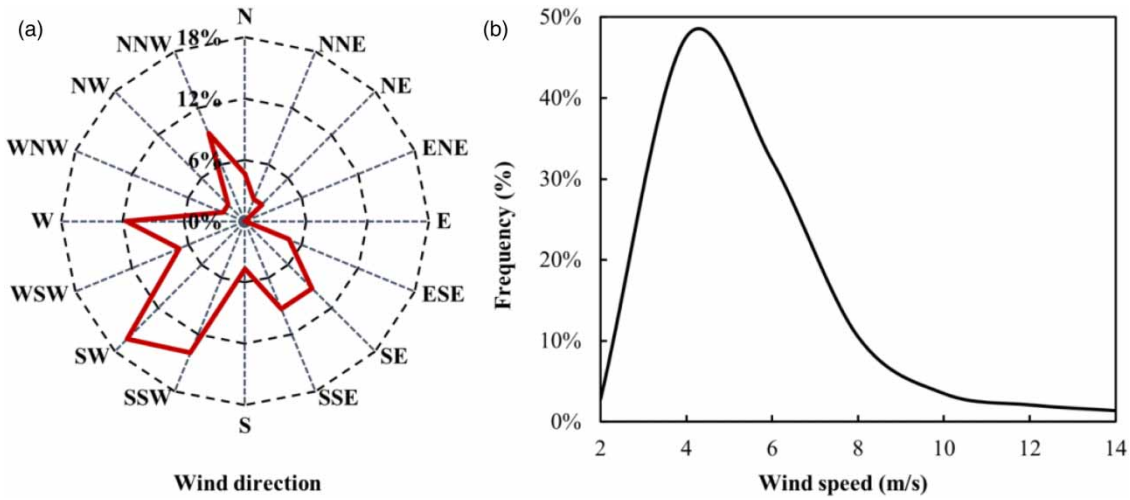

Figure 2 | The wind direction rose and the frequency of the wind speed diagram at the Boyang station in 2003, 2004, and 2007 during the backflow period.

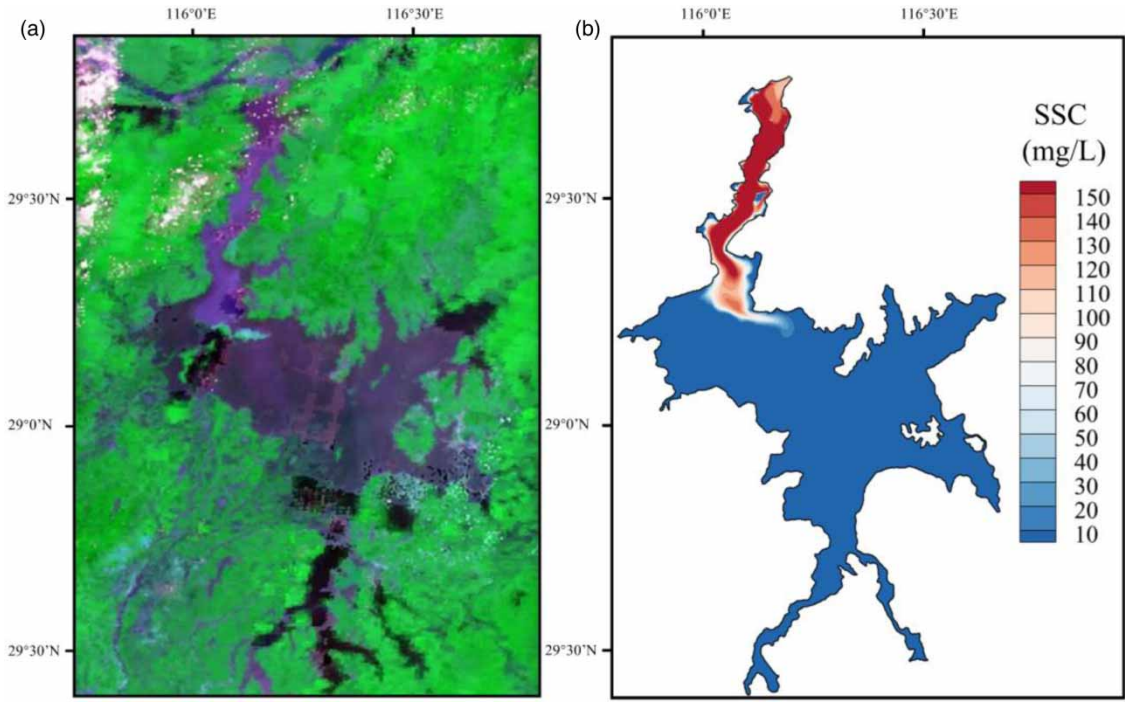

Figure 3 | (a) MODIS remote sensing before backflow. (b) Initial conditions of sediment retrieval by MODIS remote sensing.

Model evaluation

To maintain the water balance of Poyang Lake, which encompasses an area of 25,000 km^3 without station control in the catchment area, it is crucial to accurately estimate the interval flow in the uncontrolled section. The discharge of the interval flow was calibrated during the backflow periods in 2003 and 2004, which were relatively wet and dry years, respectively. The primary parameter was the runoff coefficient (α), α ranged from 0 to 1, and the initial value was set to 0.6 based on literature values (Zhang & Werner 2009; Li *et al.* 2012). A trial-and-error method was used to calibrate α using the observed lake water and outflow discharge levels at Hukou. The optimal value of α was calibrated at 0.56.

The measured water levels at the Xingzi, Duchang, Tangyin, and Kangshan stations were used to verify the hydrodynamic model in Cases 1–3. The Nash–Sutcliffe efficiency coefficient (E_{ns}) (Nash & Sutcliffe 1970), root mean square error (RMSE), and relative error (R_e) indexes were used to evaluate the water levels in Cases 1–3. Table 2 and Figure 4 show the model results and the measured water levels. The E_{ns} values ranged from 0.95 to 0.99, and the RMSE values ranged from 0.05 to 0.15 m. The R_e values of all stations were lower than 1%, suggesting a suitable agreement between the model results and field data.

Table 2 | Comparison between the model results and the field data

	Case 4			Case 5			Case 6		
Stations	R_e (%)	RMSE (m)	E_{ns}	R_e (%)	RMSE (m)	E_{ns}	R_e (%)	RMSE (m)	E_{ns}
Xingzi	0.76	0.13	0.99	0.33	0.05	0.98	0.24	0.06	0.99
Tangyin	0.55	0.13	0.99	0.09	0.06	0.98	0.06	0.07	0.99
Kangshan	0.44	0.15	0.99	−0.01	0.09	0.95	−0.05	0.09	0.99

$$R_e = \frac{\sum_{t=1}^{T}(Q_{obs}^t - Q_{sim}^t)}{\sum_{t=1}^{T} Q_{obs}^t} \times 100\%;\ \mathrm{RMSE} = \sqrt{\frac{\sum_{t=1}^{T}(Q_{obs}^t - Q_{sim}^t)^2}{T}};\quad E_{ns} = 1 - \frac{\sum_{t=1}^{T}(Q_{obs}^t - Q_{sim}^t)^2}{\sum_{t=1}^{T}(Q_{obs}^t - \overline{Q_{obs}})^2}.$$

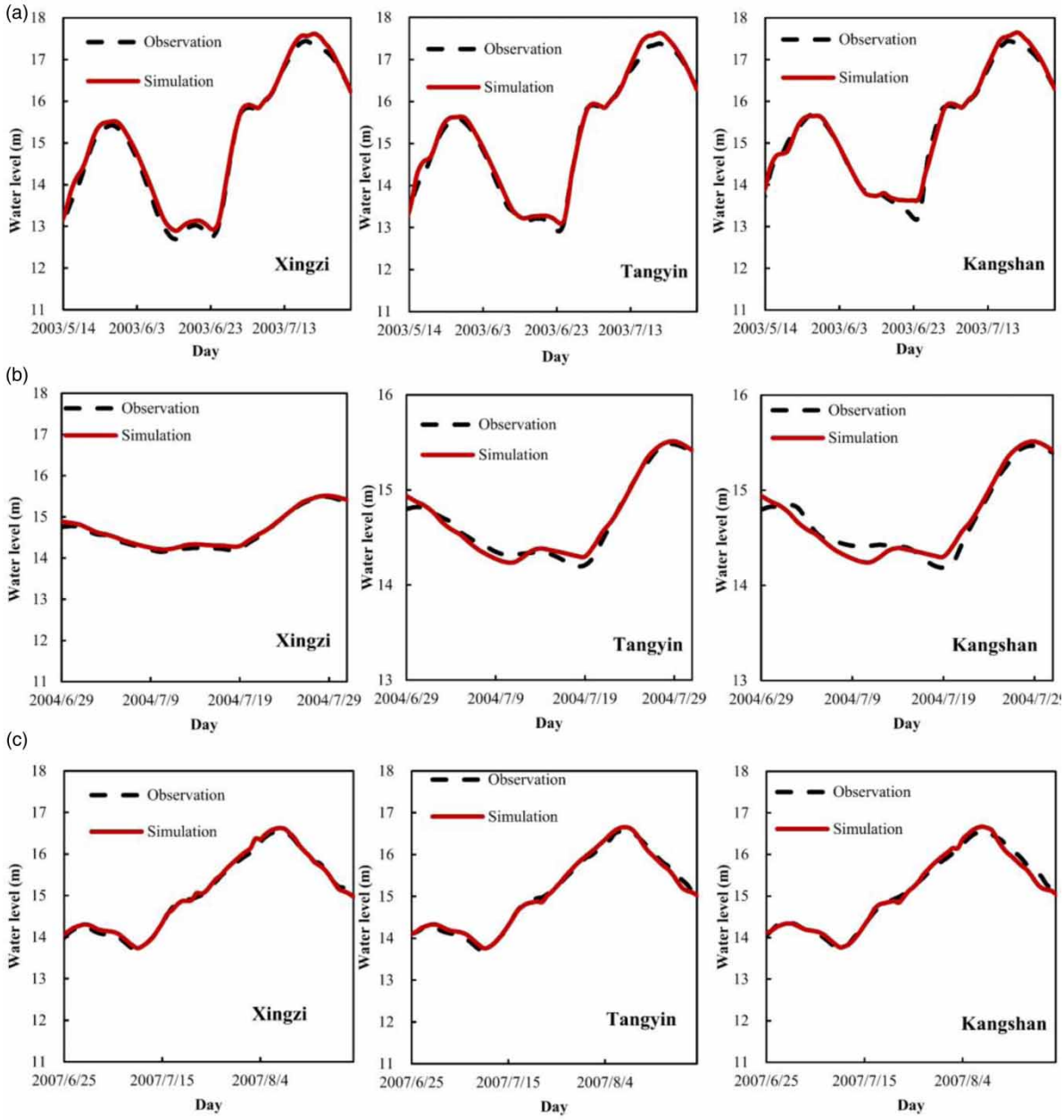

Figure 4 | Model verification of water level at the Xingzi, Tangyin, and Kangshan stations.

Figure 5 shows the sediment concentration obtained with the MODIS image and the calculated sediment concentration during the backflow periods in 2003, 2004, and 2007. The calculated sediment areas under SSW wind (Figure 5(c)) reasonably agreed with the remote sensing data, while the calculated sediment areas without wind (Figure 5(b)) were concentrated in the middle of the lake near Tangyin. In general, the FVCOM hydrodynamic model of Poyang Lake could reasonably simulate the backflow processes.

RESULTS

Flow pattern without wind during the backflow period in 2007

The operation of the Three Gorges Dam (TGD) since 2003 may have lowered the water level of the Yangtze River and reduced the backflow intensity (Li *et al.* 2017). The highest backflow after the operation occurred in 2007, which is a

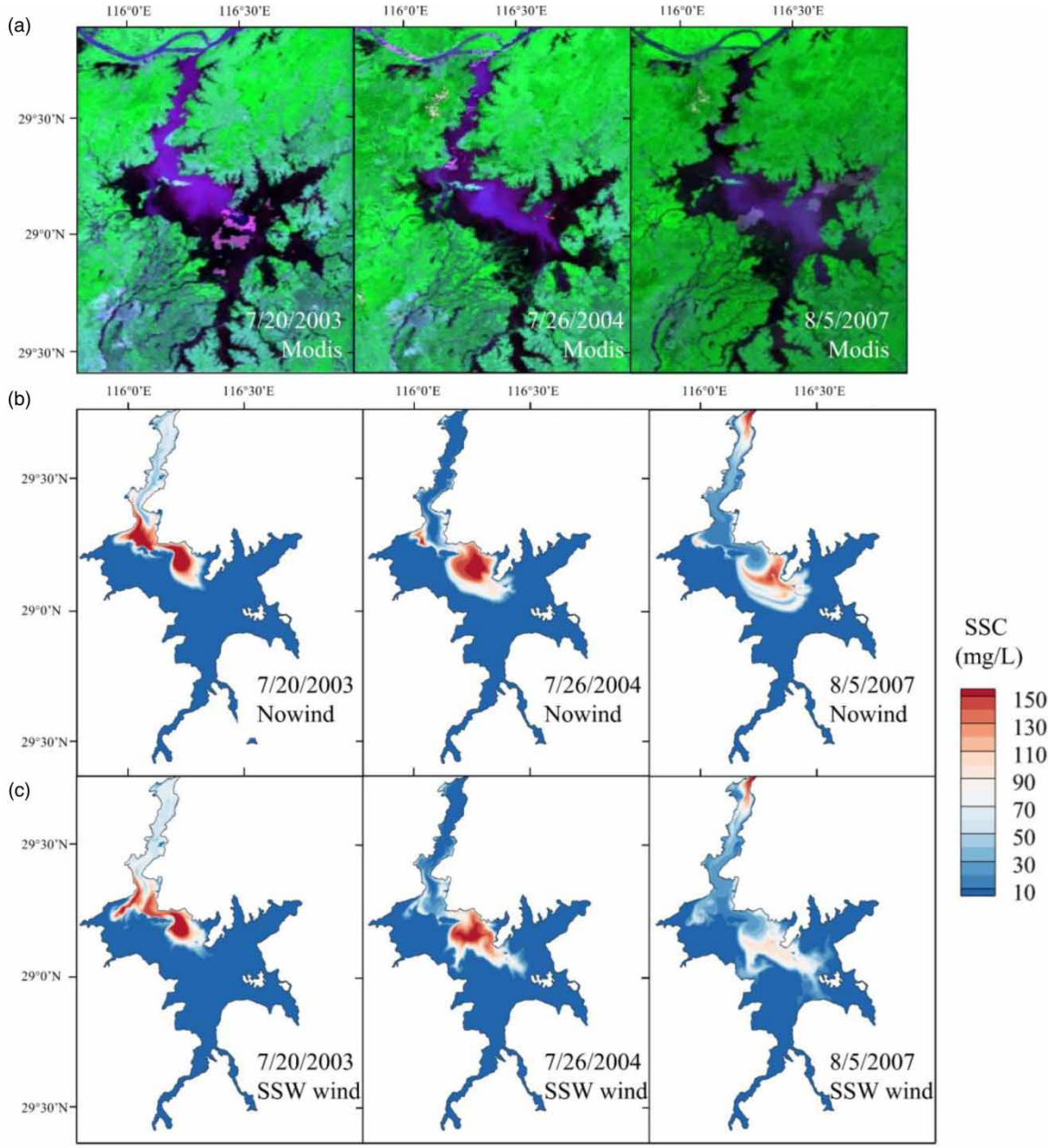

Figure 5 | Comparison between (a) MODIS image and the calculated value (b) without wind and (c) with SSW wind of sediment concentration.

representative year to explore the effects of backflow and wind forcing on lake hydrodynamics. Figure 6 shows the depth-averaged flow velocity without wind (Case 3) at the five hydrological stations, i.e., Hukou, Xingzi, Duchang, Tangyin, and Kangshan, and other two locations with different backflow discharge levels, namely, ⑥ in the western floodplain and ⑦ in the eastern bay (Figure 1). The Hukou station, which is close to the Yangtze River, experienced the greatest impact on flow velocity due to backflow discharge. In contrast, Duchang, the western floodplain, and the eastern bay were less affected by backflow discharge as they are located farther away from the Yangtze River. Additionally, there was a positive correlation between backflow discharge and velocity in the lake.

Figure 7 shows the streamlines in the lake without wind (Case 3) and with SSW (Case 6) and NNE (Case 7) winds under the 3,550 m^3/s backflow discharge, the highest discharge during the backflow period in 2007. Without wind (Case 3), the flow

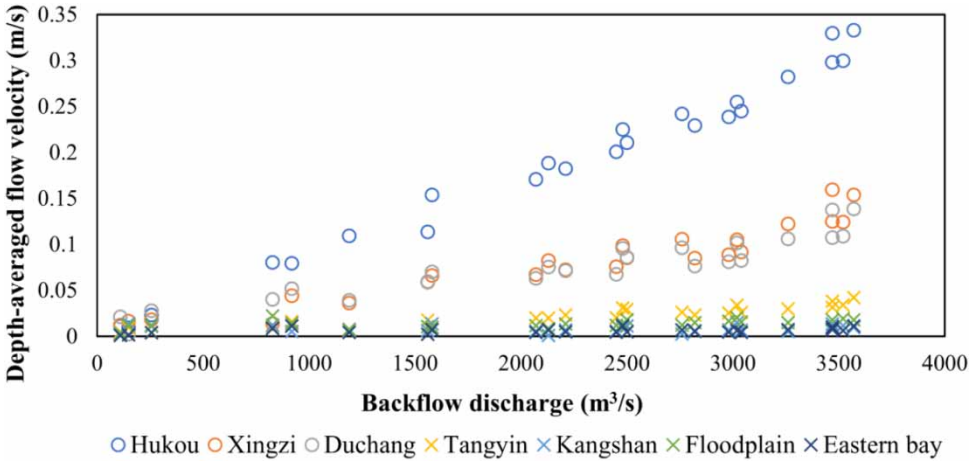

Figure 6 | Depth-averaged flow velocity at the five stations, i.e., Hukou, Xingzi, Duchang, Tangyin, Kangshan, and two locations in the western floodplain and the eastern bay with different backflow discharges without wind.

moved from Hukou to Duchang and was then divided near Tangyin. The main backflow moved to the south of the lake and the eastern bay (Figure 7(a)). The depth-averaged velocity was 0.07 m/s when the backflow entered the main lake (near Duchang) and decreased to 0.02–0.03 m/s in the middle of the lake (near Tangyin). The water in southern Tangyin was almost still, and the depth-averaged flow velocity was below 0.02 m/s.

Flow pattern with SSW wind during the backflow period in 2007

Under SSW wind (Case 6), the overall flow direction was consistent with that under no wind conditions (Case 3) in the northern channel, while in the main lake on both sides of the Tangyin–Duchang channel, gyres were found. Under the forcing of a uniform wind, the lake should develop flows in the wind direction along the shore and opposite to the wind direction in the deep area (Csanady 1973; Ji & Jin 2006). The largest gyre was around Nanshan Island in the southern lake. The terrain elevation significantly changed around Nanshan Island (Figure 1), located between the shallow floodplain and deep channel. Hence, water flowed along the relatively shallow shoal on the west side of Nanshan Island with the wind direction, and a return flow against the wind direction was observed in the relatively deep channel.

Figure 8 shows the water depth (H) in section A–A′ (orange line in Figure 7(b)) relative to the depth-averaged longitudinal velocity (v) under the 3,550 m^3/s (July 28) and 110 m^3/s (August 7) backflow discharge levels. Section A–A′ is perpendicular to the direction of the wind, and the mean depth of section A–A′, $\bar{H} = S/b$, was approximately 2.73 m on July 28. The depth-averaged longitudinal velocity was northwards in the shallow floodplain ($H > \bar{H}$) and southwards in the deep area ($H < \bar{H}$). The mean water depth line was the gyre central line, and the result is consistent with the conclusion of previous studies (Csanady 1973; Ji & Jin 2006). In addition, the depth-averaged longitudinal velocity was proportional to the water depth (H), reaching 0.05 m/s in the deep channel near Kangshan.

With continuous backflow into the lake, the mean depth ($\bar{H}$) continued to increase, and the backflow discharge decreased, resulting in expansion of the gyre area. Figure 7(c) shows the flow pattern on the last day of the backflow period. The backflow discharge decreased to 110 m^3/s, and the mean depth ($\bar{H}$) increased to approximately 4 m. The gyre area developed along the direction of the mean water depth line (orange dashed dotted line in Figure 7(c)). Another gyre was formed near Tangyin along the direction of the mean water depth line, and this gyre was separated from the gyre around Nanshan Island. Additionally, the wind-driven current from the shallow floodplain near Nanshan Island intruded into the new gyre. This result indicated that there was a boundary line between these two gyres.

Figure 7(c) shows that the boundary line between these gyres (BLG) in Poyang Lake was generated by the balance between the wind-induced current and backflow from the Yangtze River. The backflow from the Yangtze River created a water surface elevation via a pressure gradient, and the hydraulic gradient almost vanished in the Duchang–Tangyin channel without wind (Figure 9). In addition, wind forcing sets up (or down) the water surface elevation (η), and the response in a shallow lake can be quantitatively assessed using the following formula: $d\eta/dx = (\tau_x - \tau_b)/gS$, where τ_x is the wind stress along the x-direction,

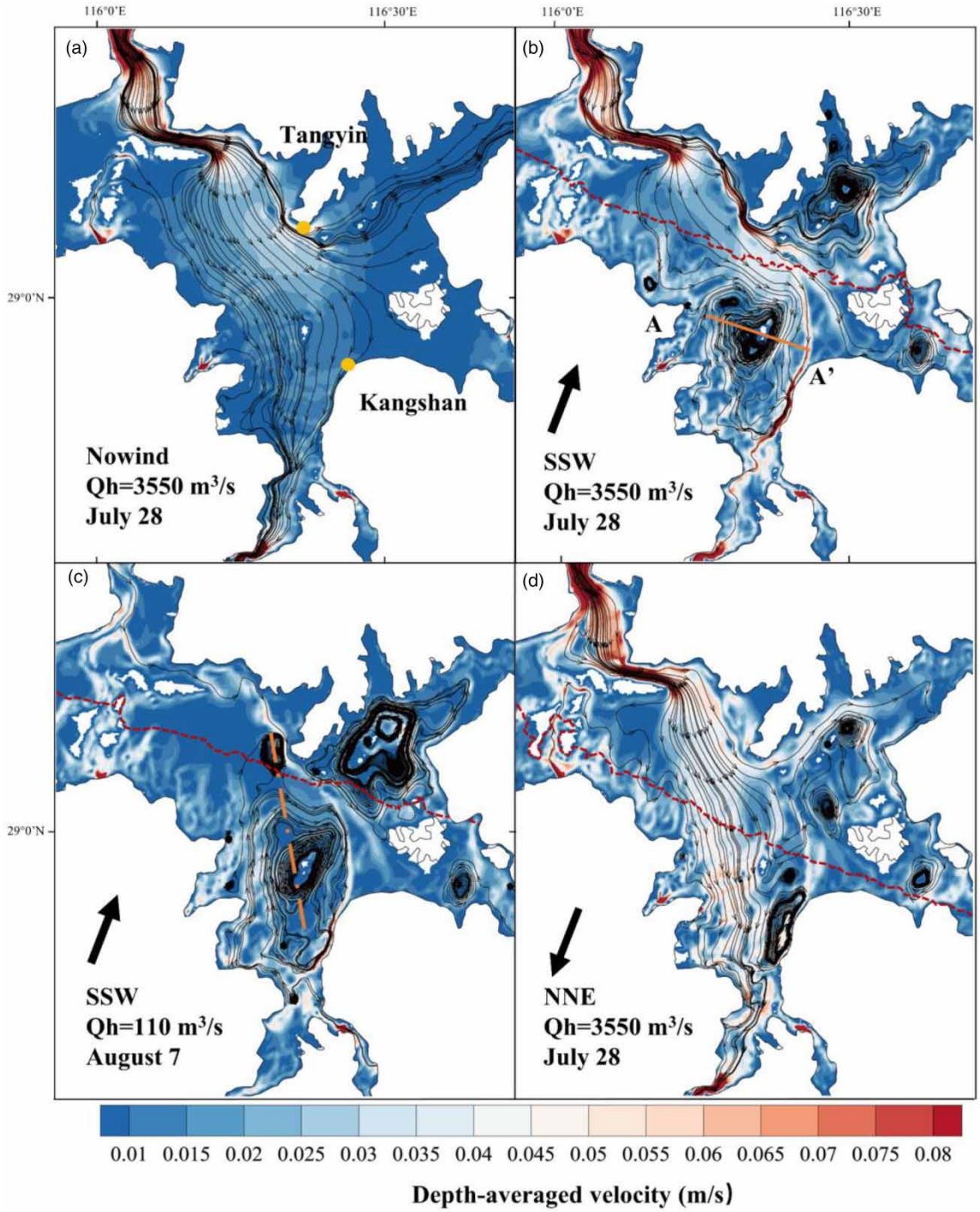

Figure 7 | Flow streamlines and depth-averaged flow velocity field (a) without wind (Case 5) on July 28 and with (b) SSW wind (Case 3) on July 28 and (c) August 7; and (d) NNE wind (Case 4) on July 28. Note that the orange dashed dot line in (c) is the mean water depth line of the gyre around Nanshan Island and the red dotted line in (b) and (c) is the line where the water surface elevation (η) value equals zero.

and τ_b is bottom shear stress along the x-direction (Csanady 1973; Ji & Jin 2006). The $\eta = 0$ line was calculated, as shown in Figures 7(b) and 8(c) (the red dotted line), where the hydraulic gradient caused by wind and backflow was zero. BLG was the $\eta = 0$ line under SSW wind. The BLG location varied relative to the mean water depth and backflow discharge, and it drifted toward near Tangyin when $\bar{H}$ increased and the backflow discharge decreased.

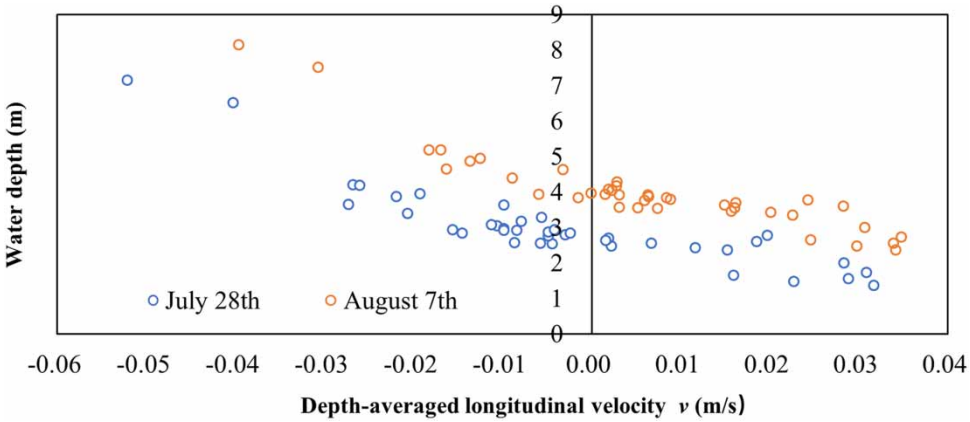

Figure 8 | Water depth (H) in section A–A′ relative to the depth-averaged longitudinal velocity (v) on July 28 under SSW wind (Case 6).

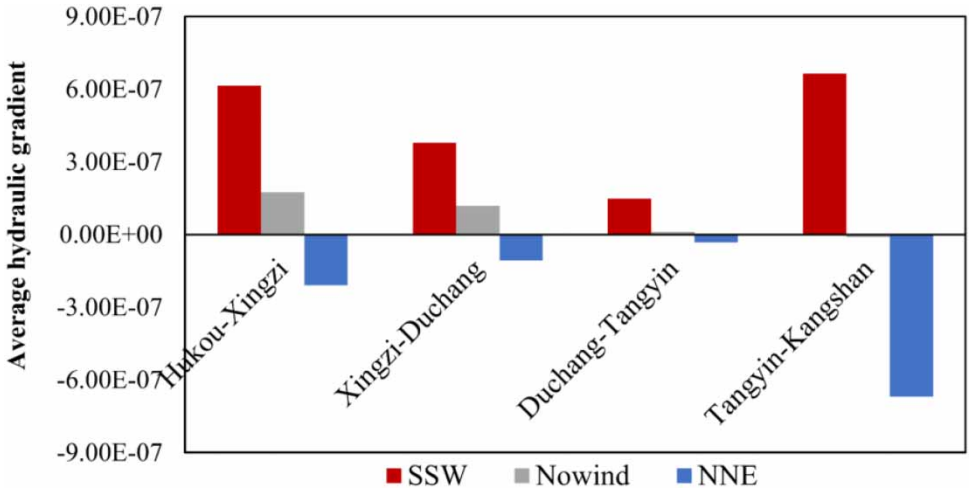

Figure 9 | Average hydraulic gradient during the backflow period of Hukou–Xingzi, Xingzi–Duchang, Duchang–Tangyin, and Tangyin–Kangshan channels without wind (Case 3) and under the SSW (Case 6) and NNE (Case 7) winds.

Flow pattern with NNE wind during the backflow period in 2007

Under NNE wind (Case 7), the $\eta = 0$ line (red dotted line in Figure 7(d)) was located in the southern lake. Wind set up the water surface elevation and accelerated the backflow southwards. The main backwater flowed southwards to the shallow floodplain and entered the tributary of the Ganjiang River. Due to the presence of the tributaries of the Ganjiang River, the southern circulation could hardly develop, resulting in the BLG line losing its guiding role.

DISCUSSION

Effect of the dominant wind on the flow pattern during the backflow period

Previous research on Poyang Lake's currents typically emphasized seasonal inflow-outflow dynamics, while wind-driven currents were often overlooked. Drawing upon the simulation results of interactions between wind-induced currents and backflow in Poyang Lake, this article provides a comprehensive overview of the three conceptual flow patterns, as shown in Figure 10. Pattern 1 shows the flow pattern without backflow, and the flow in the lake is driven by wind. The wind stress and bottom friction occurred in balance near the shallow floodplain downwind, and the BLG line was developed. The gyres occupied the entire lake, and transport occurred with the wind in the shallow portion of the lake, while return flow occurred in the deeper portion.

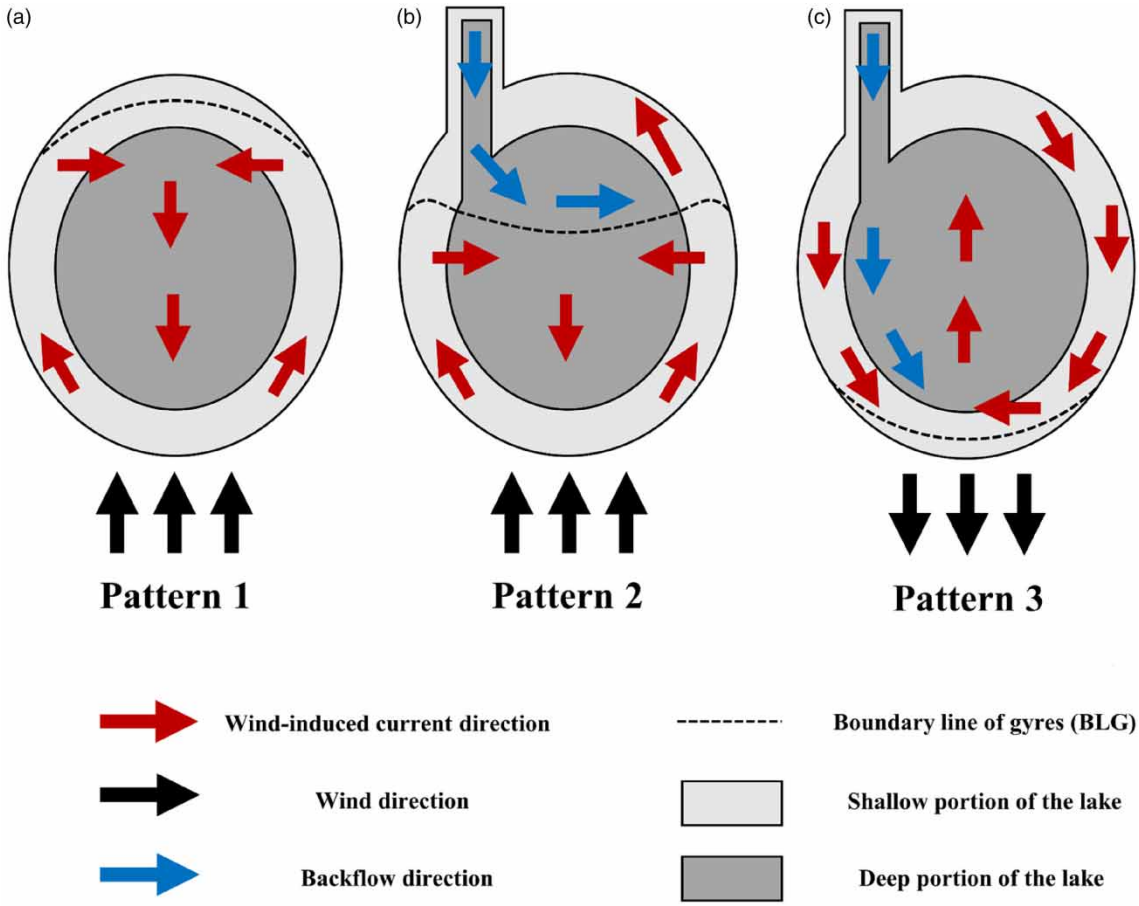

Figure 10 | Flow patterns and wind-induced currents direction under the wind and backflow.

Pattern 2 shows the flow pattern in a river-to-lake system with backflow. When the flow direction was against the wind, the hydraulic gradient caused by wind and backflow was zero, and BLG was located in the middle of the lake. Gyres formed on both sides of the BLG line, and the gyres south of the lake were similar to those in Pattern 1. The main backwater flowed along the BLG direction and merged with these gyres. When the wind direction matched the backflow direction (Pattern 3), the BLG line developed in the shallow floodplain. The main backwater moved along the shallow portion near the inlet and merged with the gyres south of the lake.

Effect of the dominant wind on sediment transport during the backflow period

In previous simulations of sediment transport during the backflow period of Poyang Lake, the impact of wind was overlooked, resulting in sediment being restricted to the centre of the lake. Nevertheless, in this study, the consideration of wind effects led to changes in the direction of lake currents, consequently altering the sediment transport processes.

The SYR distribution in these cases during the backflow period was mostly concentrated in the northern region. The average growth rate of the SYR area was 13–15 km^2 per day, and it was hardly affected by wind (not presented in this paper). Figure 11 shows the RSM distribution in Cases 3, 6, and 7 on August 7, the last day of the 2007 backflow period. Without wind (Case 3), RSM was distributed in the middle of the lake near Tangyin (Figure 11(a)), and only some RSM entered the eastern bay. Due to the low flow velocity in the Duchang–Kangshan channel (below 0.02 m/s), RSM reached the Tangyin station approximately 16 days after the backflow began and was distributed within a 13-km radius from Tangyin. The peak concentration was 130 mg/L near Tangyin, and the average growth rate of the RSM area was 11.5 km^2 per day.

Under SSW wind (Case 6), most RSM was transported along the direction of the BLG line and reached Kangshan and the eastern bay (Figure 11(b)). Due to the increased velocity under wind (approximately 0.03–0.04 m/s), RSM reached Tangyin

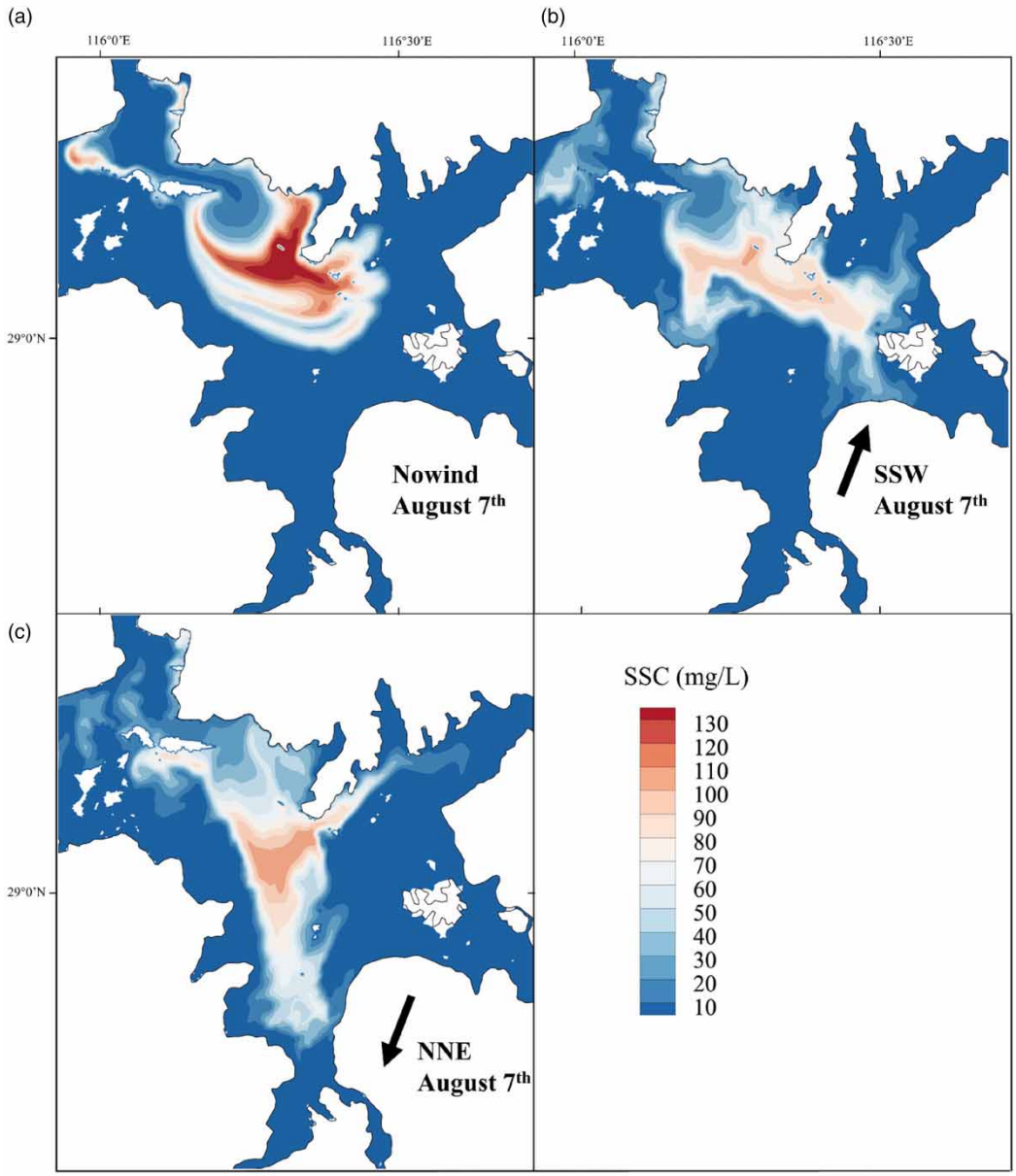

Figure 11 | RSM distribution (a) without wind and with (b) SSW and (c) NNE winds for Cases 3–5 on August 7, respectively.

and Kangshan in 12 and 18 days, respectively. The average growth rate of the RSM area was 20.1 km^2 per day, which was a 75% increase compared to the situation without wind.

Under NNE wind (Case 7), RSM moved to the shallow floodplain (Figure 11(c)), and it was distributed from Tangyin to the top south of the lake. The backflow velocity ranged from approximately 0.03 to 0.04 m/s, and it reached the top south of the lake after 17 days. The average growth rate of the RSM area was 21.3 km^2 per day, which is an 85% increase compared to the situation without wind.

Implications and limitations

Our investigation offers a more comprehensive understanding of the synergies between wind-induced currents and backflow in interconnected river–lake ecosystems. Previous studies focus on the backflow effects (Lai *et al.* 2014; Tang *et al.* 2015; Li *et al.* 2017), and our findings emphasize that, in open lake regions, the influence of wind is more pronounced than backflow.

In the context of interconnected river–lake systems, flow patterns in the constricted channels of the northern waterways are predominantly governed by backflow. In contrast, in the expansive central lake regions, flow patterns are dominated by the wind, which largely shapes the overall hydrodynamics of the lake. This detailed understanding would lead to more informed management and conservation strategies tailored to the specific needs of the different lake regions.

Building upon the analysis of water flow patterns, this study further elucidates the primary factors governing sediment transport. Previous studies suggested that sediment within the northern inlet channel of Poyang Lake could enter the lake area during backflow (Cui *et al.* 2009, 2013). However, this viewpoint may need to be revised. The findings of this study indicate that backflow currents can only transport suspended sediment to the central area of the lake, while sediment entering the upstream region is primarily influenced by wind. This study has provided clear insights into the contributions and mechanisms of various factors in sediment transport. By examining the influence of wind on backflow and sediment dynamics in Poyang Lake, our study offers a foundation for future sand mining schemes, as a significant source of sediment is sand mining activities. Delving deeper into this relationship in future research could further enhance the management and preservation of the lake's aquatic environment.

The model was based on certain assumptions and simplifications. First and foremost, while our study assessed the effects of wind forcing based on two primary directions of uniform prevailing wind, it was crucial to acknowledge that real-world wind forcing had far more intricate spatial and temporal variations (Greatbatch & Goulding 1989; Hwang 2005). Especially during periods of weaker winds, a large fluctuation in wind direction was observed. Moreover, the landscape's complex topography had a significant role in determining wind variability. The shifts from one dominant wind direction to another could bring about intricate modifications in the flow field (Jalil *et al.* 2017). Furthermore, spatial inconsistencies in wind could also introduce variations in flow patterns (Huang *et al.* 2016). Although our research primarily focused on gauging the effects of commonly occurring wind conditions, future studies should reveal the detailed spatiotemporal dynamics of the wind field. Additionally, our simulation of sediment transport took into account boundary conditions pegged to the peak backflow volume post-completion of the TGD. However, the study did not explore the several scenarios stemming from variations in backflow volumes, nor did it investigate its influence on the hydrodynamic attributes of the lake's backflow. This remains a pertinent avenue for future research.

CONCLUSION

This study investigated the synergistic effects of hydraulic and wind forces on hydrodynamics and sediment transportation in the Yangtze River–Poyang Lake system during backflow in Poyang Lake. A numerical model was utilized and validated by field data and MODIS remote sensing data. The outcomes of this study offer significant insights and a novel approach to the ecological management of the Yangtze River and Poyang Lake. The following conclusions can be drawn:

(1) This investigation was the first to investigate the interplay between backflow and wind-induced currents in Poyang Lake. Through a comprehensive analysis, the study sheds light on the influence of the wind on flow patterns and sediment transport.
(2) Using numerical simulations, the research mapped out the depth-averaged flow velocities at key hydrological stations within the lake, revealing a positive correlation between backflow discharge and velocity. This correlation is more pronounced from the center of the lake to Hukou, while it is not evident in the upstream regions of the lake.
(3) The study demonstrated the pivotal role of wind in shaping the flow patterns and sediment transport processes in the lake. Without wind influence, the backflow follows a relatively predictable path from Hukou to Duchang, dividing near Tangyin. However, introducing wind forces from dominant directions modifies the overall flow direction and instigates the formation of gyres, significantly impacting the sediment transport routes.
(4) Our findings underscore the importance of wind-induced currents in the sediment transport process during the backflow period. The sediment transport mechanisms, previously believed to be primarily influenced by backflow, are found to be deeply intertwined with wind forces in Poyang Lake. This newfound understanding underscores the necessity of re-evaluating sediment transport theories within the context of Poyang Lake.

Poyang Lake's hydrodynamics and sediment transport are markedly shaped by wind fields, highlighting the need for improved wind monitoring. Wind-driven sediment transport can stress ecologically sensitive areas, calling for targeted protection and restoration. Moreover, a further scope is to explore the impact of changes in backflow volume and water level

on the hydrodynamics. Notably, after the operation of the TGD, changes in the backflow volume and water level features have been observed.

AUTHOR CONTRIBUTIONS

All authors contributed to the research conception and design. Material preparation, data collection, and analysis were performed by Y.Y., S.Y., H.C., and C.J. Y.Y. wrote the first draft of the manuscript and all authors commented on previous versions of the manuscript. All authors read and approved the final manuscript.

FUNDING

This research was funded by the National Key R&D Program of China (2022YFC3202602), the National Natural Science Foundation of China (U2040205; 52079044), the Fok Ying Tung Education Foundation (520013312), and the 111 Project (B17015).

CONSENT TO PARTICIPATE

All authors confirm their co-authorship.

CONSENT TO PUBLISH

The authors give their consent for the publication of this manuscript.

DATA AVAILABILITY STATEMENT

All relevant data are included in the paper or its Supplementary Information.

CONFLICT OF INTEREST

The authors declare there is no conflict.

REFERENCES

Ayele, G. T., Kuriqi, A., Jemberrie, M. A., Saia, S. M., Seka, A. M., Teshale, E. Z., Daba, M. H., Ahmad Bhat, S., Demissie, S. S., Jeong, J. & Melesse, A. M. 2021 Sediment yield and reservoir sedimentation in highly dynamic watersheds: the case of Koga Reservoir, Ethiopia. *Water* **13** (23), 3374. https://doi.org/10.3390/w13233374.

Chen, C., Liu, H. & Beardsley, R. C. 2003 An unstructured grid, finite-volume, three-dimensional, primitive equations ocean model: application to coastal ocean and estuaries. *Journal of Atmospheric and Oceanic Technology* **20** (1), 159–186. https://doi.org/10.1175/1520-0426(2003)020<0159:AUGFVT>2.0.CO;2.

Chen, C., Huang, H., Beardsley, R. C., Liu, H., Xu, Q. & Cowles, G. 2007 A finite volume numerical approach for coastal ocean circulation studies: comparisons with finite difference models. *Journal of Geophysical Research: Oceans* **112** (C3). https://doi.org/10.1029/2006JC003485.

Chen, L., Jin, Z., Michishita, R., Cai, J., Yue, T., Chen, B. & Xu, B. 2014 Dynamic monitoring of wetland cover changes using time-series remote sensing imagery. *Ecological Informatics* **24**, 17–26. https://doi.org/10.1016/j.ecoinf.2014.06.007.

Csanady, G. T. 1973 Wind-induced barotropic motions in long lakes. *Journal of Physical Oceanography* **3** (4), 429–438. https://doi.org/10.1175/1520-0485(1973)003<0429:WIBMIL>2.0.CO;2.

Cui, L., Wu, G. & Liu, Y. 2009 Monitoring the impact of backflow and dredging on water clarity using MODIS images of Poyang Lake, China. *Hydrological Processes* **23** (2), 342–350. https://doi.org/10.1002/hyp.7163.

Cui, L., Qiu, Y., Fei, T., Liu, Y. & Wu, G. 2013 Using remotely sensed suspended sediment concentration variation to improve management of Poyang Lake, China. *Lake and Reservoir Management* **29** (1), 47–60. https://doi.org/10.1080/10402381.2013.768733.

Deoli, V., Kumar, D. & Kuriqi, A. 2022 Detection of water spread area changes in eutrophic lake using landsat data. *Sensors* **22** (18), 6827. https://doi.org/10.3390/s22186827.

Feng, L., Hu, C., Chen, X., Cai, X., Tian, L. & Gan, W. 2012 Assessment of inundation changes of Poyang Lake using MODIS observations between 2000 and 2010. *Remote Sensing of Environment* **121**, 80–92. https://doi.org/10.1016/j.rse.2012.01.014.

Galperin, B., Kantha, L. H., Hassid, S. & Rosati, A. 1988 A quasi-equilibrium turbulent energy model for geophysical flows. *Journal of the Atmospheric Sciences* **45** (1). https://doi.org/10.1175/1520-0469(1988)045<0055:AQETEM>2.0.CO;2.

Greatbatch, R. J. & Goulding, A. 1989 Seasonal variations in a linear barotropic model of the North Pacific driven by the Hellerman and Rosenstein wind stress field. *Journal of Geophysical Research: Oceans* **94** (C9), 12645–12665. https://doi.org/10.1029/JC094iC09p12645.

Guo, H., Hu, Q., Zhang, Q. & Feng, S. 2012 Effects of the three gorges dam on Yangtze river flow and river interaction with Poyang Lake, China: 2003–2008. *Journal of Hydrology* **416**, 19–27. https://doi.org/10.1016/j.jhydrol.2011.11.027.

Hu, Q., Feng, S., Guo, H., Chen, G. & Jiang, T. 2007 Interactions of the Yangtze river flow and hydrologic processes of the Poyang Lake, China. *Journal of Hydrology* **347** (1–2), 90–100. https://doi.org/10.1016/j.jhydrol.2007.09.005.

Huang, L., Fang, H., He, G., Jiang, H. & Wang, C. 2016 Effects of internal loading on phosphorus distribution in the Taihu Lake driven by wind waves and lake currents. *Environmental Pollution* **219**, 760–773. https://doi.org/10.1016/j.envpol.2016.07.049.

Hwang, P. A. 2005 Temporal and spatial variation of the drag coefficient of a developing sea under steady wind-forcing. *Journal of Geophysical Research: Oceans* **110** (C7). https://doi.org/10.1029/2005JC002912.

Jalil, A., Li, Y., Du, W., Wang, J., Gao, X., Wang, W. & Acharya, K. 2017 Wind-induced flow velocity effects on nutrient concentrations at Eastern Bay of Lake Taihu, China. *Environmental Science and Pollution Research* **24**, 17900–17911. https://doi.org/10.1007/s11356-017-9374-x.

Ji, Z. G. & Jin, K. R. 2006 Gyres and seiches in a large and shallow lake. *Journal of Great Lakes Research* **32** (4), 764–775. https://doi.org/10.3394/0380-1330(2006)32[764:GASIAL]2.0.CO;2.

Jiang, H., Liu, Y. & Lu, J. 2021 A new algorithm for monitoring backflow from river to lake (BRL) using satellite images: a case of Poyang Lake, China. *Water* **13** (9), 1166. https://doi.org/10.3390/w13091166.

Khan, M. Y. A., Hasan, F. & Tian, F. 2019a Estimation of suspended sediment load using three neural network algorithms in Ramganga River catchment of Ganga Basin, India. *Sustainable Water Resources Management* **5**, 1115–1131. https://doi.org/10.1007/s40899-018-0288-7.

Khan, M. Y. A., Tian, F., Hasan, F. & Chakrapani, G. J. 2019b Artificial neural network simulation for prediction of suspended sediment concentration in the River Ramganga, Ganges Basin, India. *International Journal of Sediment Research* **34** (2), 95–107. https://doi.org/10.1016/j.ijsrc.2018.09.001.

Kumar, M., Kumar, P., Kumar, A., Elbeltagi, A. & Kuriqi, A. 2022 Modeling stage–discharge–sediment using support vector machine and artificial neural network coupled with wavelet transform. *Applied Water Science* **12** (5), 87. https://doi.org/10.1007/s13201-022-01621-7.

Lai, X., Shankman, D., Huber, C., Yesou, H., Huang, Q. & Jiang, J. 2014 Sand mining and increasing Poyang Lake's discharge ability: a reassessment of causes for lake decline in China. *Journal of Hydrology* **519**, 1698–1706. https://doi.org/10.1016/j.jhydrol.2014.09.058.

Li, X. H., Zhang, Q. & Xu, C. Y. 2012 Suitability of the TRMM satellite rainfalls in driving a distributed hydrological model for water balance computations in Xinjiang catchment, Poyang Lake basin. *Journal of Hydrology* **426**, 28–38. https://doi.org/10.1016/j.jhydrol.2012.01.013.

Li, Y., Zhang, Q., Yao, J., Werner, A. D. & Li, X. 2014 Hydrodynamic and hydrological modeling of the Poyang Lake catchment system in China. *Journal of Hydrologic Engineering* **19** (3), 607–616. https://doi.org/10.1061/(ASCE)HE.1943-5584.0000835.

Li, Y., Zhang, Q., Werner, A. D., Yao, J. & Ye, X. 2017 The influence of river-to-lake backflow on the hydrodynamics of a large floodplain lake system (Poyang Lake, China). *Hydrological Processes* **31** (1), 117–132. https://doi.org/10.1002/hyp.10979.

Li, Y., Khan, M. Y. A., Jiang, Y., Tian, F., Liao, W., Fu, S. & He, C. 2019 CART and PSO + KNN algorithms to estimate the impact of water level change on water quality in Poyang Lake, China. *Arabian Journal of Geosciences* **12**, 1–12. https://doi.org/10.1007/s12517-019-4350-z.

Li, Y., Zhang, Q., Liu, X. & Yao, J. 2020 Water balance and flashiness for a large floodplain system: a case study of Poyang Lake, China. *Science of the Total Environment* **710**, 135499. https://doi.org/10.1016/j.scitotenv.2019.135499.

Liu, X., Li, Y. L., Liu, B. G., Qian, K. M., Chen, Y. W. & Gao, J. F. 2016 Cyanobacteria in the complex river-connected Poyang Lake: horizontal distribution and transport. *Hydrobiologia* **768**, 95–110. https://doi.org/10.1007/s10750-015-2536-2.

Liu, H., Li, Q., Shi, T., Hu, S., Wu, G. & Zhou, Q. 2017 Application of sentinel 2 MSI images to retrieve suspended particulate matter concentrations in Poyang Lake. *Remote Sensing* **9** (7), 761. https://doi.org/10.3390/rs9070761.

Liu, X., Zhang, Q., Li, Y., Tan, Z. & Werner, A. D. 2020 Satellite image-based investigation of the seasonal variations in the hydrological connectivity of a large floodplain (Poyang Lake, China). *Journal of Hydrology* **585**, 124810. https://doi.org/10.1016/j.jhydrol.2020.124810.

Ma, Y., Xiong, C. & Yi, W. 2003 Sedimentary characteristics and developing trend of sediments in Poyang Lake, Jiangxi province. *Resources Survey & Environment* **24** (1), 29–37 (in Chinese). http://dx.doi.org/10.3969/j.issn.1671-4814.2003.01.005.

Mei, X., Dai, Z., Du, J. & Chen, J. 2015 Linkage between Three Gorges Dam impacts and the dramatic recessions in China's largest freshwater lake, Poyang Lake. *Scientific Reports* **5** (1), 18197. https://doi.org/10.1038/srep18197.

Mellor, G. L. & Yamada, T. 1982 Development of a turbulence closure model for geophysical fluid problems. *Reviews of Geophysics* **20** (4), 851–875. https://doi.org/10.1029/RG020i004p00851.

Mu, S., Li, B., Yao, J., Yang, G., Wan, R. & Xu, X. 2020 Monitoring the spatio-temporal dynamics of the wetland vegetation in Poyang Lake by Landsat and MODIS observations. *Science of the Total Environment* **725**, 138096. https://doi.org/10.1016/j.scitotenv.2020.138096.

Nash, J. E. & Sutcliffe, J. V. 1970 River flow forecasting through conceptual models part I – a discussion of principles. *Journal of Hydrology* **10** (3), 282–290. https://doi.org/10.1016/0022-1694(70)90255-6.

Shankman, D., Keim, B. D. & Song, J. 2006 Flood frequency in China's Poyang Lake region: trends and teleconnections. *International Journal of Climatology* **26** (9), 1255–1266. https://doi.org/10.1002/joc.1307.

Smagorinsky, J. 1963 General circulation experiments with the primitive equations: I. The basic experiment. *Monthly Weather Review* **91** (3), 99–164. https://doi.org/10.1175/1520-0493(1963)091<0099:GCEWTP>2.3.CO;2.

Tang, C. X., Xiong, X., Wu, N. H., Zhang, X. H. & Zou, W. N. 2015 Simulation of the impact of the reverse flow from Yangtze River on the hydrodynamic process of Lake Poyang. *Journal of Lake Sciences* **27** (4), 700–710 (in Chinese with English Abstr.). https://doi.org/10.18307/2015.0419.

Tang, H., Cao, H., Yuan, S., Xiao, Y., Jiang, C. & Gualtieri, C. 2020 A numerical study of hydrodynamic processes and flood mitigation in a large river-lake system. *Water Resources Management* **34**, 3739–3760. https://doi.org/10.1007/s11269-020-02628-y.

Wang, P., Lai, G. & Li, L. 2015 Predicting the hydrological impacts of the Poyang Lake project using an EFDC model. *Journal of Hydrologic Engineering* **20** (12), 05015009. https://doi.org/10.1061/(ASCE)HE.1943-5584.0001240.

Wang, Y., Kao, Y. C., Zhou, Y., Zhang, H., Yu, X. & Lei, G. 2019 Can water level management, stock enhancement, and fishery restriction offset negative effects of hydrological changes on the four major Chinese carps in China's largest freshwater lake? *Ecological Modelling* **403**, 1–10. https://doi.org/10.1016/j.ecolmodel.2019.03.020.

Wang, H., Kaisam, J. P., Liang, D., Deng, Y. & Shen, Y. 2020 Wind impacts on suspended sediment transport in the largest freshwater lake of China. *Hydrology Research* **51** (4), 815–832. https://doi.org/10.2166/nh.2020.153.

Wu, G., de Leeuw, J., Skidmore, A. K., Prins, H. H. & Liu, Y. 2007 Concurrent monitoring of vessels and water turbidity enhances the strength of evidence in remotely sensed dredging impact assessment. *Water Research* **41** (15), 3271–3280. https://doi.org/10.1016/j.watres.2007.05.018.

Xu, L., Yuan, S., Tang, H., Qiu, J., Xiao, Y., Whittaker, C. & Gualtieri, C. 2022 Mixing dynamics at the large confluence between the Yangtze River and Poyang Lake. *Water Resources Research* **58** (11), e2022WR032195. https://doi.org/10.1029/2022WR032195.

Yang, G., Zhang, Q., Wan, R., Lai, X., Jiang, X., Li, L., Dai, H., Lei, Guang., Chen, J. & Lu, Y. 2016 Lake hydrology, water quality and ecology impacts of altered river–lake interactions: advances in research on the middle Yangtze river. *Hydrology Research* **47** (S1), 1–7. https://doi.org/10.2166/nh.2016.003.

Yao, J., Zhang, Q., Li, Y. L. & Li, M. 2016 The influence of uniform winds on hydrodynamics of Lake Poyang. *Journal of Lake Sciences* **28** (1), 225–236 (in Chinese with English Abstr.). https://doi.org/10.18307/2016.0126.

Yao, J., Zhang, Q., Ye, X., Zhang, D. & Bai, P. 2018 Quantifying the impact of bathymetric changes on the hydrological regimes in a large floodplain lake: Poyang Lake. *Journal of Hydrology* **561**, 711–723. https://doi.org/10.1016/j.jhydrol.2018.04.035.

Yao, J., Li, Y., Zhang, D., Zhang, Q. & Tao, J. 2019 Wind effects on hydrodynamics and implications for ecology in a hydraulically dominated river-lake floodplain system: Poyang Lake. *Journal of Hydrology* **571**, 103–113. https://doi.org/10.1016/j.jhydrol.2019.01.057.

Yuan, S., Tang, H., Xiao, Y., Qiu, X. & Xia, Y. 2018 Water flow and sediment transport at open-channel confluences: an experimental study. *Journal of Hydraulic Research* **56** (3), 333–350. https://doi.org/10.1080/00221686.2017.1354932.

Yuan, S., Tang, H., Li, K., Xu, L., Xiao, Y., Gualtieri, C., Rennie, C. & Melville, B. 2021 Hydrodynamics, sediment transport and morphological features at the confluence between the Yangtze River and the Poyang Lake. *Water Resources Research* **57** (3), e2020WR028284. https://doi.org/10.1029/2020WR028284.

Zhang, Q. & Werner, A. D. 2009 Integrated surface–subsurface modeling of Fuxianhu Lake catchment, Southwest China. *Water Resources Management* **23**, 2189–2204. https://doi.org/10.1007/s11269-008-9377-y.

Zhang, S., Liu, Y., Yang, Y., Sun, C. & Li, F. 2016 Erosion and deposition within Poyang Lake: evidence from a decade of satellite data. *Journal of Great Lakes Research* **42** (2), 364–374. https://doi.org/10.1016/j.jglr.2015.12.012.

Zou, H., Zhang, S., Liu, Y., Zhang, W. & Yang, X. 2020 Analysis of a convective storm crossing Poyang Lake in China. *Journal of Meteorological Research* **34** (3), 529–545. https://doi.org/10.1007/s13351-020-9143-5.

First received 5 June 2023; accepted in revised form 28 September 2023. Available online 11 October 2023